Neurosci. Bull. October, 2018, 34(5):715–724
https://doi.org/10.1007/s12264-018-0266-y

www.neurosci.cn
www.springer.com/12264

ORIGINAL ARTICLE

Abnormal Metabolic Connectivity in Rats at the Acute Stage of Ischemic Stroke

Shengxiang Liang[1,2,5] · Xiaofeng Jiang[6] · Qingqing Zhang[5] · Shaofeng Duan[2,3] · Tianhao Zhang[2,3] · Qi Huang[2,3] · Xi Sun[1,2] · Hua Liu[2,3] · Jie Dong[1] · Weilin Liu[5] · Jing Tao[5] · Shujun Zhao[1] · Binbin Nie[2,3,4] · Lidian Chen[5] · Baoci Shan[2,3,4]

Received: 14 November 2017 / Accepted: 18 May 2018 / Published online: 6 August 2018

Abstract Stroke at the acute stage is a major cause of disability in adults, and is associated with dysfunction of brain networks. However, the mechanisms underlying changes in brain connectivity in stroke are far from fully elucidated. In the present study, we investigated brain metabolism and metabolic connectivity in a rat ischemic stroke model of middle cerebral artery occlusion (MCAO) at the acute stage using ^{18}F-fluorodeoxyglucose positron emission tomography. Voxel-wise analysis showed decreased metabolism mainly in the ipsilesional hemisphere, and increased metabolism mainly in the contralesional cerebellum. We used further metabolic connectivity analysis to explore the brain metabolic network in MCAO. Compared to sham controls, rats with MCAO showed most significantly reduced nodal and local efficiency in the ipsilesional striatum. In addition, the MCAO group showed decreased metabolic central connection of the ipsilesional striatum with the ipsilesional cerebellum, ipsilesional hippocampus, and bilateral hypothalamus. Taken together, the present study demonstrated abnormal metabolic connectivity in rats at the acute stage of ischemic stroke, which might provide insight into clinical research.

Keywords Ischemic stroke · FDG PET · Metabolic connectivity · Acute

Introduction

Stroke affects an estimate of 17 million people each year globally [1], and > 80% of patients suffer motor disability after stroke [2]. On account of the importance of diagnosis and treatment at the acute stage for recovery after stroke, many studies have investigated the pathogenesis, diagnosis, and treatment of stroke at the acute stage [3–5]. However, many issues have yet to be elucidated. A number of studies have focused on the functional network of stroke at the acute stage using functional magnetic resonance (fMRI) [6–8]. Resting functional connectivity in the motor network is altered in patients with stroke at the acute stage compared to healthy controls [8]. In a previous study, we also found that the alleviation of neurological deficits is associated with the improvement of abnormal networks after stroke [9]. Thus, understanding of the functional connectivity of the brain at the acute stage could be useful for the diagnosis and treatment of stroke.

Functional connectivity, which can be interpreted as neural interactivity and assessed by fMRI [10, 11] and positron emission tomography (PET) [12], is defined by statistical association or dependency between brain

✉ Shujun Zhao
zhaosj@zzu.edu.cn

✉ Binbin Nie
niebb@ihep.ac.cn

1 College of Physical Science and Technology, Zhengzhou University, Zhengzhou 450001, China

2 Beijing Engineering Research Center of Radiographic Techniques and Equipment, Institute of High Energy Physics, Chinese Academy of Sciences, Beijing 100049, China

3 School of Nuclear Science and Technology, University of Chinese Academy of Sciences, Beijing 100049, China

4 CAS Center for Excellence in Brain Science and Intelligence Technology, Shanghai Institutes for Biological Sciences, Chinese Academy of Sciences, Shanghai 200031, China

5 College of Rehabilitation Medicine, Fujian University of Traditional Chinese Medicine, Fuzhou 350122, China

6 School of Public Health and Family Medicine, Capital Medical University, Beijing 100068, China

regions. While the fMRI-based functional connectivity estimates the correlation of fast temporal fluctuations [13], metabolic connectivity measured by ^{18}F-fluorodeoxyglucose (^{18}F-FDG) PET reflects cumulative energy consumption and provides information on the presumed steady resting state [12, 14]. Metabolic connectivity could be a critical complement to understanding functional connectivity and provides valuable insights into the pathophysiology of disorders. However, few studies have investigated the metabolic connectivity of stroke at the acute stage.

As the brain is a complex integrative system, the properties of disordered networks are usually assessed *via* graph theory to further explore their characteristics in brain disorders such as Alzheimer's disease [15, 16], Parkinson's disease [17], and stroke [18, 19]. Although several studies have examined topographic changes in the acute stage of stroke [18, 20], few have investigated the characteristics of the metabolic network at this stage. One study has reported alterations in brain connectivity features in the acute stage of stroke using fMRI [20]. Besides, the characteristics of cortical connectivity changes in the acute stage stroke have been measured using cortical sources of electroencephalography [18]. Graph theory could be an effective method for understanding the features of brain metabolic connectivity as a complex system in the acute stage of stroke.

With the aim to explore brain metabolic connectivity in the acute stage of stroke, we applied FDG-PET to assess metabolic connectivity and used graph theory to estimate its features in a rat ischemic stroke model of middle cerebral artery occlusion (MCAO).

Materials and Methods

Animals

Healthy male Sprague-Dawley rats, weighing 280 ± 20 g, were provided by Shanghai Laboratory Animal Co., Ltd., Shanghai, China (license no. SCXK 2014-0005) and housed under controlled environmental conditions (12:12 h light:dark cycle, ambient temperature 23 ± 2 °C and 60%–70% humidity). The rats were food-restricted to maintain 85%–90% of their free-feeding weight (10 g/day–15 g/day) before operation. All protocols were approved by the Committee on Animal Care and Usage of Fujian University of Traditional Chinese Medicine, and all the protocols were in accord with the Chinese Specifications in the Care and Use of the Laboratory Animals (SPF animal laboratory). All efforts were made to minimize animal suffering. According to the random number table method, rats were randomly and evenly separated into 2 groups: the sham-operated control group (SC group, n = 9), and the MCAO group (n = 9).

Focal Cerebral Ischemia Reperfusion Model

The rat model was induced by transient MCAO on the left side for 2 h followed by reperfusion. The detailed procedure was as described by Longa *et al.* [21]. Briefly, the rats were anesthetized with 3% isoflurane in 67% N_2O and 30% O_2. MCAO on the left side was performed using an occluding suture with an embolus (Jia Ling embolus; Jia Ling Biological Technology Ltd., Guangzhou, China) for 2 h, and the suture was slowly withdrawn to allow reperfusion after 2 h of MCAO-induced cerebral ischemia. The ipsilateral cerebral blood flow (CBF) was measured by laser Doppler flowmetry (Biopac Systems, Goleta, CA). The MCAO model was considered successful only when CBF dropped to become equal to or > 80% of the baseline during occlusion. The sham-operated rats underwent identical surgical procedures, except that the intraluminal filament was not inserted. Physiological parameters were monitored throughout the surgery. Rectal temperature was maintained at 37 °C until the rats recovered from anesthesia. After surgery and recovery, the animals were maintained at room temperature. One of nine rats in the MCAO group died after operation. All the rats were deprived of food for 12 h–15 h before ^{18}F-FDG injection, but had access to drinking water at any time.

PET Scans

^{18}F-FDG was prepared at the PET Center of the China PLA General Hospital. For each rat, ^{18}F-FDG (18.5 MBq/100 g body weight) was injected *via* tail vein without anesthesia. Then the rats were kept in cages and placed in a room with minimal ambient noise for ^{18}F-FDG uptake. The uptake period was 40 min for maximization of ^{18}F-FDG uptake by the brain [22]. Then the rats were anesthetized by isoflurane inhalation (2% in 100% oxygen; IsoFlo: Hebei Jiumu Phama, Ltd, China) using a nose cone.

Nine rats in the sham group and eight in the MCAO group underwent FDG-PET scans. Twelve hours after operation, FDG-PET images were acquired on a micro PET system (E-plus166, Institute of High Energy Physics, Chinese Academy of Sciences, China), which had a radial spatial resolution of 1.67 mm full-width at half-maximum at the center of the field of view. For FDG-PET scan, all the rats were anesthetized with isoflurane (as above) and placed prone in the scanner with a plastic stereotactic head holder on the scanner bed. The brain was centered in the field of view for static acquisition of 30 min. Images were subsequently reconstructed using a filtered back-projection algorithm. Images were reconstructed on a 128 × 128 × 63 matrix, where the voxel size was 0.5 × 0.5 × 1 mm^3. All scans were saved in Analyze format.

Image Preprocessing

All preprocessing was performed using Statistical Parametric Mapping8 (SPM8, Wellcome Department of Clinical Neurology, London, UK) with the spmratIHEP plugin [23–25]. First, all images were spatially normalized into Paxinos and Watson space [26], comprising scaling up the voxel size by a factor of 4 in each dimension, registering to the FDG-PET template, subsequently removing extracranial tissues *via* the intracranial image, and shearing the matrix to cut off the background. Then, all the normalized images were smoothed by a Gaussian kernel of $2 \times 2 \times 4$ mm^3 full-width at half-maximum. For scaling voxel intensities, the voxel counts were normalized by an optimal factor in each PET image [27].

Voxel-Wise Comparison of MCAO and Sham Groups

The two-sample *t*-test was performed voxel-by-voxel to determine the FDG uptake differences in the whole brain between the MCAO and sham groups. Regions with significant FDG changes in rats with MCAO were yielded based on a voxel-level height threshold of $P < 0.05$ (family-wise error (FWE) corrected) and a cluster-extent threshold of 50 voxels.

Construction of Connectivity Matrix

To generate the brain network, 32 anatomical volumes of interest (VOIs) (Table 1) were selected as nodes. The VOIs, which were cortical and subcortical structures as well as the cerebellum, were predefined by a 3D digital map based on the Paxinos and Watson atlas [23, 26]. Intensity-normalized FDG uptake in the VOIs of each rat was obtained. Pearson's correlation coefficients between each pair of VOIs were calculated in an inter-subject manner. A weighted undirected network matrix (32×32) was constructed for the MCAO and sham groups, in which the strength of each connection was defined as a correlation coefficient [28].

Graph Theory Analysis

On the basis of the weighted undirected network, distance matrixes [29, 30] of the MCAO and sham groups were generated. The distance between nodes was defined as:

$$d_{ij} = 1 - w_{ij}$$

where w_{ij} is the connection weight between nodes i and j.

Graph theoretical approaches using the Brain Connectivity Toolbox (https://sites.google.com/site/bctnet/) [30] were applied to characterize the functional connectivity patterns in the MCAO and sham groups. The global efficiency (E_{global}) and characteristic path length (L_{network}) were used to assess the global network properties [28, 30, 31], where E_{global} is the harmonic mean of the minimum path length between all possible pairs of nodes in the network and L_{network} is the average shortest path length for each node. They were defined as:

$$E_{\text{global}}(G) = \frac{1}{N(N-1)} \sum_{i \neq j \in G} \frac{1}{L_{i,j}}$$

and

$$L_{\text{network}}(G) = \frac{1}{N(N-1)} \sum_{i \neq j \in G} L_{i,j}$$

where $L_{i,j}$ is the shortest path length between nodes i and j, and N is the number of nodes in a graph (G).

Nodal efficiency (E_{nodal}) and local efficiency (E_{local}) were evaluated for each node to assess the regional network properties [19, 30], where E_{nodal} is an inverse of the harmonic mean of the minimum path length between a given node and other nodes in the network and E_{local} is the global efficiency of subgraphs of the neighbors of a given node. They were defined as:

$$E_{\text{nodal}}(i) = \frac{1}{N-1} \sum_{i \neq j \in G} \frac{1}{L_{i,j}}$$

and

Table 1 List of volumes of interest.

Number	Region name	Abbreviation
1	Olfactory cortex	Ent
2	Parietal association cortex	PtA
3	Amygdaloid body	Amy
4	Auditory cortex	A
5	Cerebellum	CB
6	Cingulate gyrus	Cg
7	Hippocampus	Hip
8	Hypothalamus	HTha
9	Insular cortex	IC
10	Motor cortex	MC
11	Parietal cortex posterior area	P
12	Retrosplenial cortex	RSC
13	Somatosensory cortex	S
14	Striatum	CS
15	Thalamus	Tha
16	Visual cortex	V

$$E_{\text{local}}(G_i)=\frac{1}{N_G(N_G-1)}\sum_{j,k\in G}\frac{1}{L_{j,k}}$$

where N_G is the number of nodes in the subgraph G_i, and the subgraph G_i is the network that contains the neighboring nodes of node i.

Permutation tests were repeated 10000 times to assess statistical differences in the network parameters E_{global}, E_{nodal}, and E_{local}. $P < 0.05$ was considered statistically significant.

Statistical Analysis

Permutation tests were performed to statistically compare the network matrixes in the MCAO and sham groups. The network matrixes of the MCAO and sham groups were transformed to Z scores using Fisher transformation. The images were randomly permuted 10000 times into pseudo-random groups and the network matrixes were calculated. Then, all the network matrixes were transformed by Fisher transformation. Type I errors were determined by comparison of the observed Z score for each connection with the Z score distribution from the permuted data. The false discovery rate (FDR) was applied to correct for multiple comparisons at a threshold of $q < 0.05$.

Results

Glucose Metabolism Changes in the MCAO Group

The location of the lesion in the acute stage in MCAO is displayed in Fig. 1A, and the regions of infarct as assessed by PET included decreased metabolic activity in the striatum, auditory cortex, and somatosensory cortex (Fig. 1B). Voxel-wise comparisons were performed to evaluate significant differences in metabolic activity between the MCAO and sham groups. To illustrate the significant differences, the results were overlaid on a magnetic resonance T2-weighted image of a rat brain in Paxinos and Watson space (Fig. 1C). Compared with the sham group, the MCAO group showed hypo-metabolism in the ipsilesional striatum, ipsilesional somatosensory cortex, ipsilesional auditory cortex, ipsilesional thalamus, bilateral amygdaloid body, ipsilesional insular cortex, ipsilesional hippocampus, and bilateral olfactory cortex (Fig. 1C). On the other hand, the MCAO group showed hyper-metabolism in the contralesional somatosensory cortex, contralesional auditory cortex, contralesional thalamus, contralesional parietal cortex posterior area, contralesional hippocampus, contralesional visual cortex, bilateral retrosplenial cortex, and bilateral cerebellum (Fig. 1C).

Characteristic Global and Regional Graph Theory Measures in the MCAO Group

To further investigate brain function in the MCAO group at the acute stage, metabolic connectivity was assessed in an inter-subject manner, in order to reflect inter-regional covariance patterns of neuronal activity. Correlation matrixes representing the connection strength of pairwise VOIs and connectivity graphs were constructed for the sham (Fig. 2A) and MCAO (Fig. 2B) groups. The connectivity of each group was visualized as a connectivity graph for the sham (Fig. 2C) and MCAO (Fig. 2D) groups. The overall connectivity in the MCAO group was lower than that in the sham group (Fig. 2A–D).

Graph theory was used to further investigate the network parameters in the MCAO and sham groups. Compared with the sham group, the MCAO group showed significantly decreased E_{global} ($P < 0.001$, Fig. 3A) and increased L_{network} ($P < 0.001$, Fig. 3B) global network parameters. Compared to the sham group, the MCAO group showed decreased E_{nodal} and E_{local} local network parameters in most nodes, whereas these parameters in the contralesional somatosensory cortex, contralesional auditory cortex, contralesional hippocampus, contralesional olfactory cortex, and contralesional thalamus showed increases in the MCAO group, in which the FDG uptake increased (Fig. 4A and B). Among the differences in the nodes between the MCAO and sham groups, the difference in E_{nodal} and E_{local} of the ipsilesional striatum was the highest ($P < 0.001$, Fig. 4A and B). The differences of E_{nodal} and E_{local} for anatomical localization and regional graph measures are displayed in Fig. 4C and D.

Metabolic Connectivity Decreased in the MCAO Group

Significantly decreased connectivity between pairwise VOIs in the MCAO group was found using permutation tests (Fig. 5A) and visualized as a connectivity graph (Fig. 5B). Significantly decreased metabolic connectivity in the ipsilesional striatum with the ipsilesional cerebellum, ipsilesional hippocampus, and bilateral hypothalamus was found using permutation tests.

Discussion

In the present study, a large-scale brain network based on glucose metabolic usage measured by FDG-PET was applied to evaluate the metabolic connectivity in the acute stage of MCAO. Voxel-wise analysis showed decreased metabolism mainly in the ipsilesional hemisphere and increased metabolism mainly in the contralesional

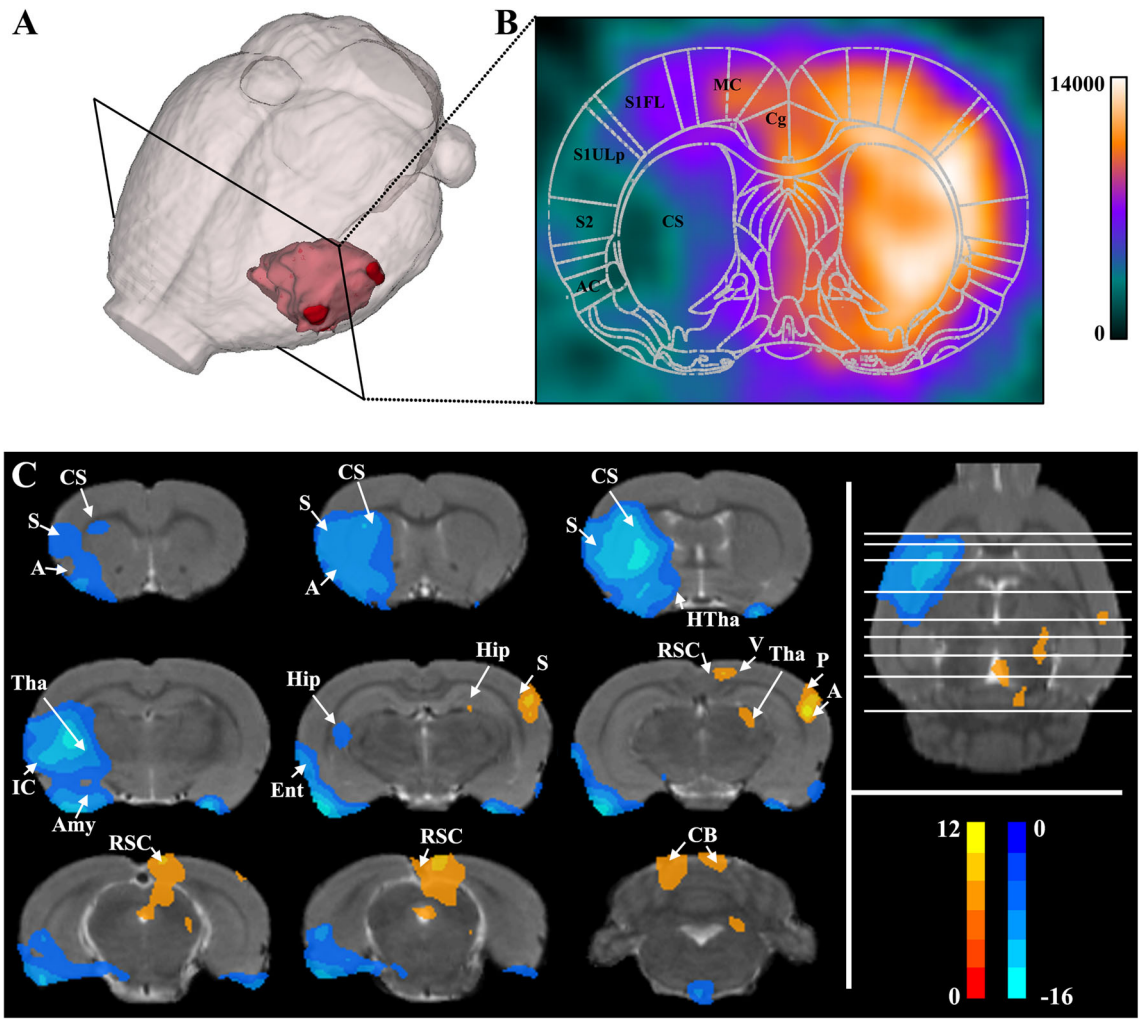

Fig. 1 Changes of glucose metabolism in the MCAO group. **A**, **B** Location of lesion in the acute stage of MCAO. Color bar indicates FDG uptake values. **C** Voxel-wise comparison of MCAO and sham groups ($P < 0.05$, FWE corrected and clusters > 50 voxels). MCAO group: $n = 8$, SC group: $n = 9$. A, auditory cortex; Amy, amygdaloid body; CB, cerebellum; CS, striatum; Ent, olfactory cortex; Hip, hippocampus; HTha, hypothalamus; IC, insular cortex; P, parietal cortex posterior area; RSC, retrosplenial cortex; S, somatosensory cortex; Tha, thalamus; V visual cortex.

cerebellum in the MCAO group. Further connectivity analysis using VOIs showed significantly lower connection strength in the MCAO group than in the sham group. Graph theoretic analysis based on the metabolic connection implied that the global and regional networks changed in the MCAO group compared to the sham group. E_{global} in the MCAO group was significantly lower and $L_{network}$ in the MCAO was significantly higher than those in the sham group. Although E_{nodal} and E_{local} of most nodes were decreased in the MCAO group, E_{nodal} and E_{local} of several nodes in the MCAO group were increased in the contralesional olfactory cortex, contralesional auditory cortex, contralesional hippocampus, contralesional somatosensory cortex, and contralesional thalamus. And the difference in E_{nodal} and E_{local} of the ipsilesional striatum between the MCAO and sham groups was the highest. Furthermore, an abnormal metabolic connection at the ipsilesional striatum with the ipsilesional cerebellum, ipsilesional hippocampus and bilateral hypothalamus in the acute stage of MCAO was found.

Voxel-wise comparison showed that the functional deficits in the MCAO rats were mainly associated with the ipsilesional hemisphere, as generally accepted. The functional deficits in motor cortex, somatosensory cortex, striatum, thalamus, amygdaloid body, and auditory cortex of the MCAO rats might be associated with the infarction of the ipsilesional hemisphere. These results are consistent with previous animal [32, 33] and clinical experiments [8]. The motor cortex, somatosensory cortex, and caudate-putamen are known to be involved in gaze, orientation, and motor skills [34–37], so the functional deficits in these regions would contribute to the motor dysfunction in

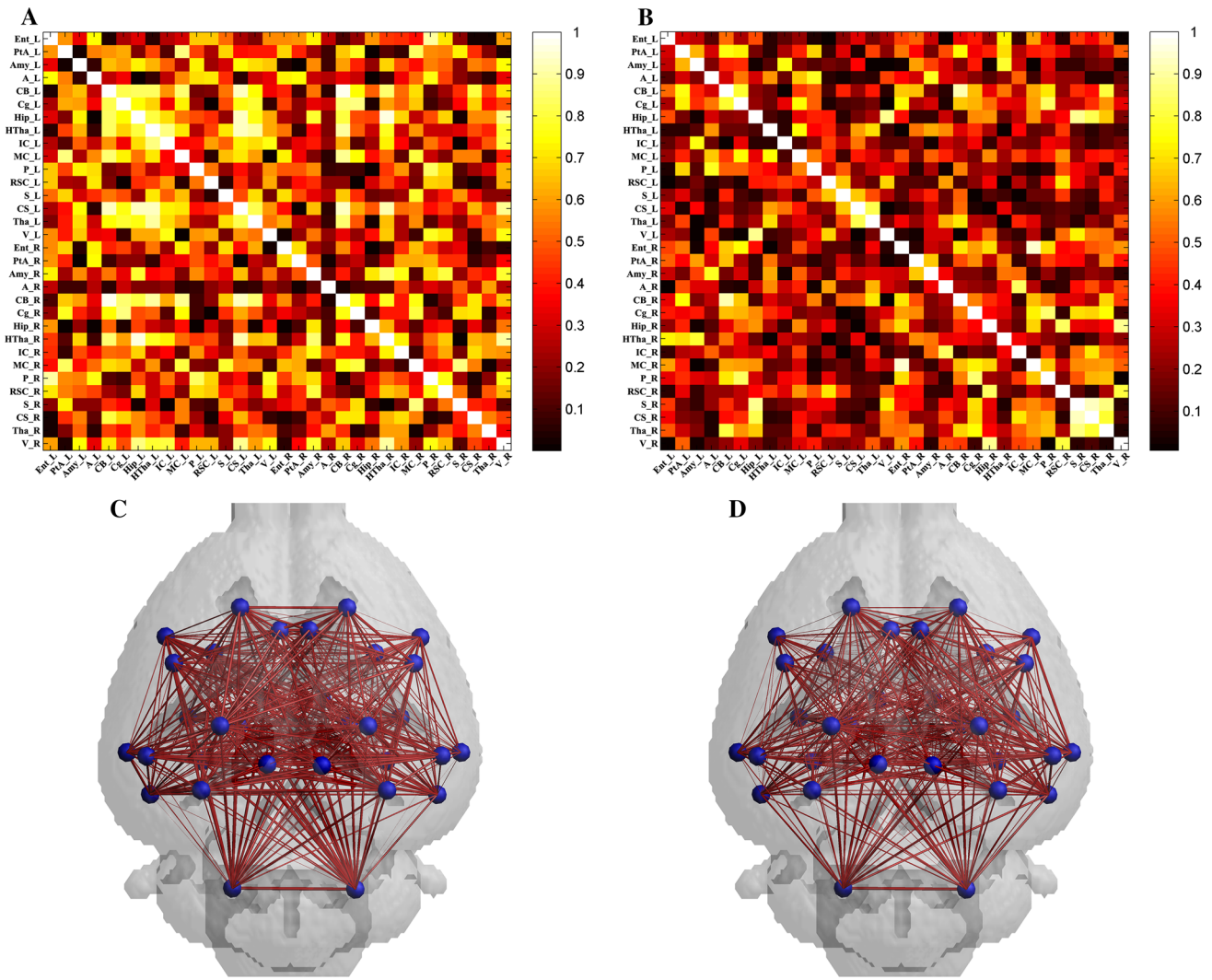

Fig. 2 Metabolic correlation networks of the sham and MCAO groups. **A** and **C** Connectivity matrix (**A**) and connectivity graph (**C**) of the sham group (n = 9). **B** and **D** Connectivity matrix (**B**) and connectivity graph (**D**) of the MCAO group (n = 8).

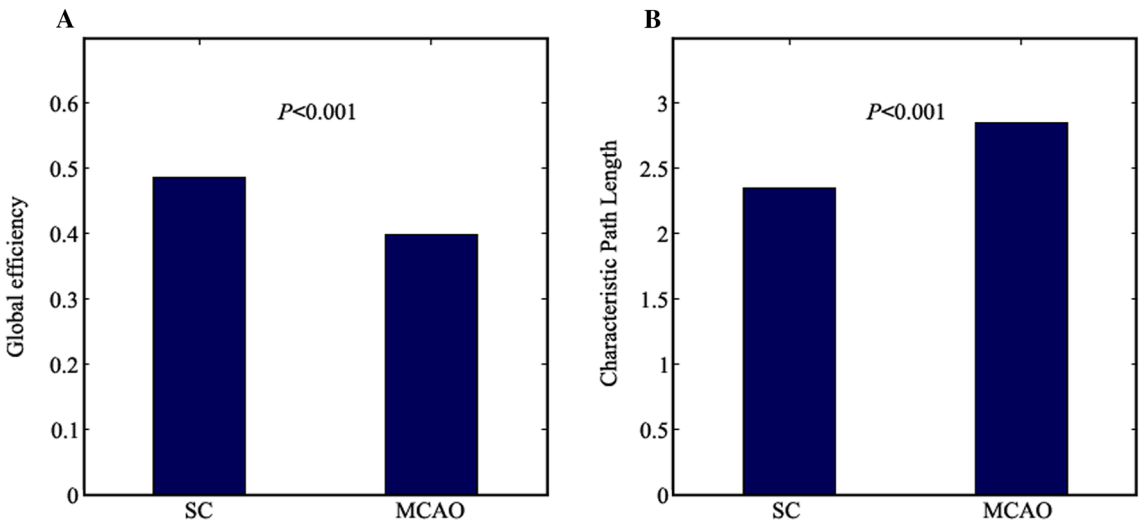

Fig. 3 Global graph theoretic measures. Global efficiency (**A**) and characteristic path length (**B**) in the MCAO (n = 8) and sham (n = 9) groups using permutation tests.

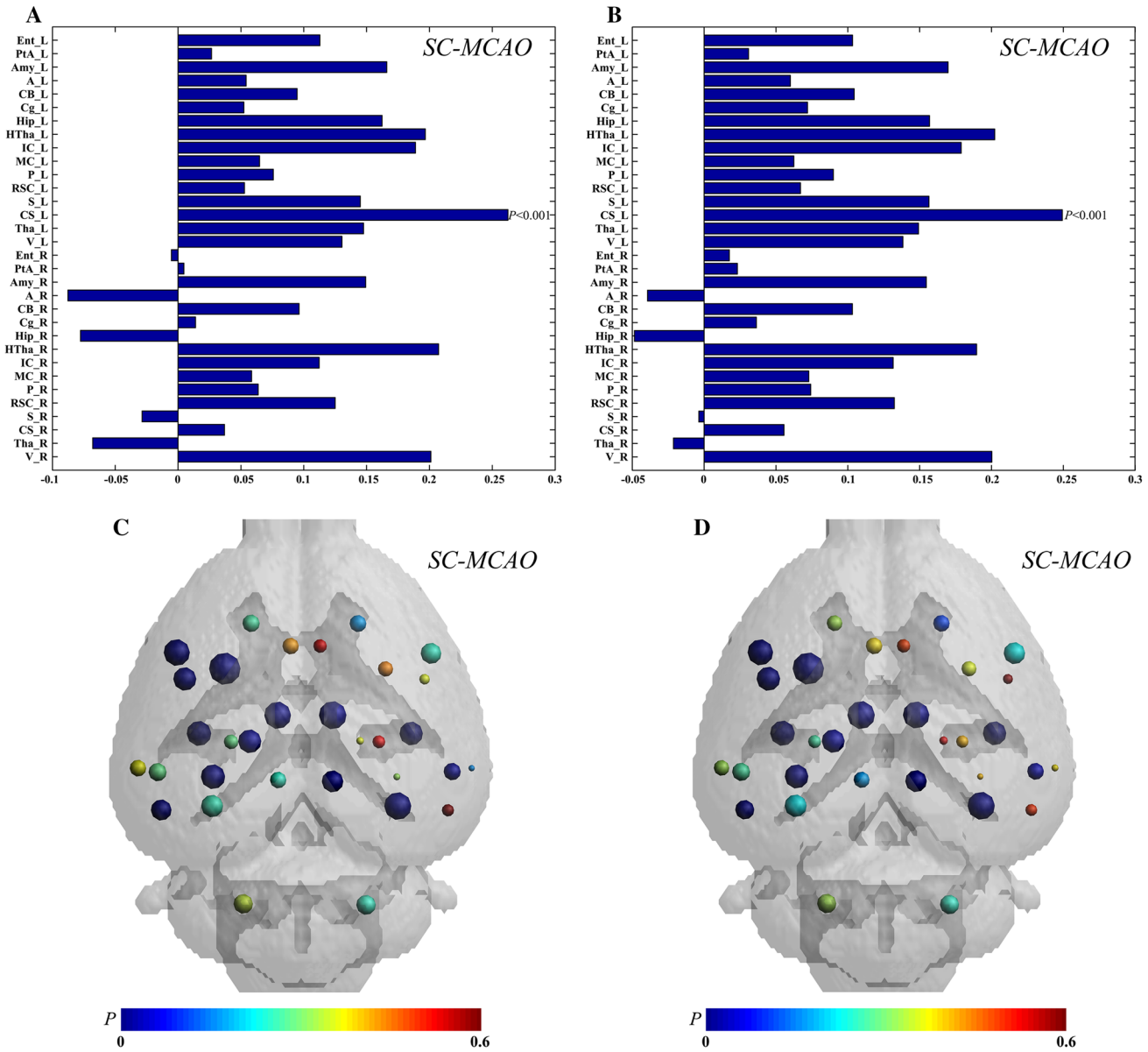

Fig. 4 Regional graph theoretic measures. Differences of nodal efficiency (**A**) and local efficiency (**B**) for each node between the MCAO and sham groups. The largest difference was found in the ipsilesional striatum. The differences of nodes in nodal efficiency (**C**) and local efficiency (**D**) between the MCAO and sham groups are displayed in Paxinos and Watson space. The sizes of nodes represent differences between the MCAO and sham groups, and the colors of nodes represent *P* values. MCAO group, $n = 8$; SC group, $n = 9$.

ischemic stroke [38, 39]. Furthermore, the results showed that functional activity was higher in the contralesional motor cortex, somatosensory cortex, thalamus, retrosplenial cortex, and auditory cortex of the MCAO rats than in the sham rats. Several studies have shown increased activation in the contralesional hemisphere following a lesion in the acute stage, which is related to somatosensory processing and motor performance [40–42]. The role of the contralesional hemisphere might be influenced by the lesion volume, and is involved in functional alterations after a stroke. A number of studies have proposed that inhibition of the contralesional hemisphere improves the motor performance after stroke [42, 43]. The contralesional hemisphere activity might play a negative role in the functional recovery after ischemic stroke.

Analysis of the metabolic network is based on the coupling of neuronal activity and brain metabolism, which can be measured by PET [12, 14]. As the FDG-PET reflects the cumulative energy consumption during awake and steady states even in animals, the PET-based metabolic network plays a complementary role in investigating brain functional connectivity. Several studies have applied the metabolic network to investigate the dysfunction in brain disorders, such as Alzheimer's dementia [15] and epilepsy

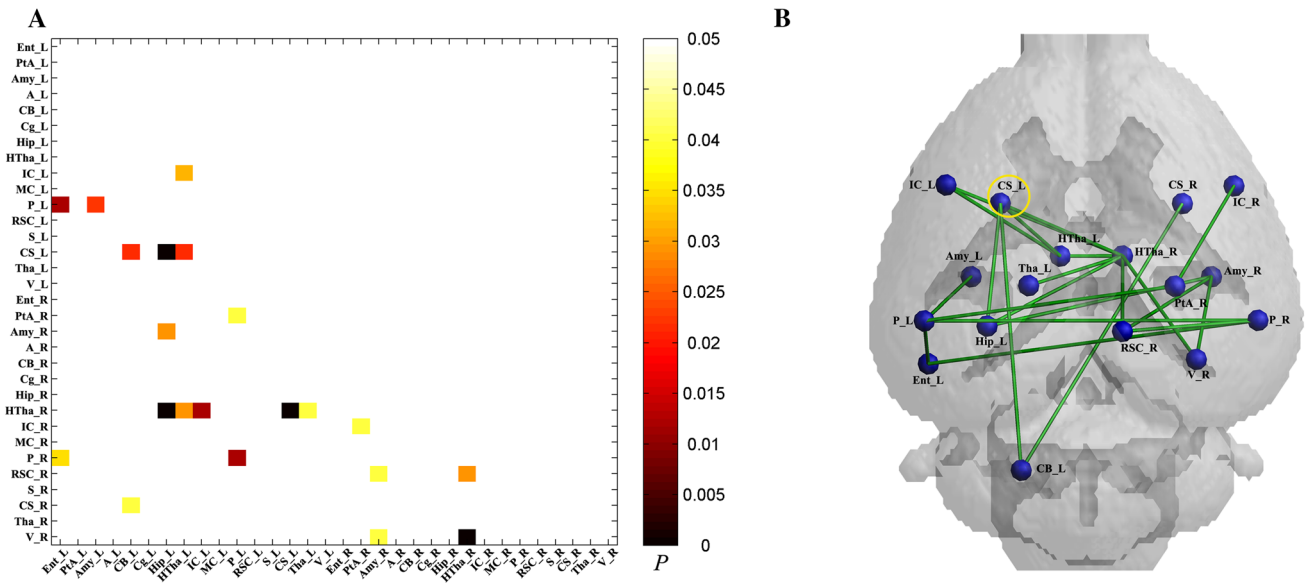

Fig. 5 Metabolic connectivity in the MCAO ($n = 8$) and sham ($n = 9$) groups. **A** Significant differences in metabolic connectivity between the MCAO and sham groups using permutation tests ($P < 0.05$ with FDR correction). Compared to the sham group, statistical significance of decreased metabolic connectivity in the MCAO group was found and represented by lower triangular matrix. **B** Anatomical distribution of significantly different metabolic connections in pairwise VOIs between the MCAO and sham groups.

[29]. We described the brain dysfunction at the acute stage of MCAO as revealed by voxel-wise comparison analysis, similar to previous studies [8, 33]. Based on the previous studies [29], the number of rats in our study was appropriate. Analysis of the metabolic network in MCAO contributes to understanding the mechanisms underlying abnormal functional connectivity at the acute stage of stroke.

Analysis of the metabolic network showed that the overall connectivity of pairs VOIs was decreased in the acute stage of MCAO. And significantly decreased global efficiency and increased characteristic path length were found in the MCAO group compared to the sham group. A lower global efficiency is predominantly associated with weaker capacity of the network for parallel information transfer between nodes *via* multiple series of edges [31], while a longer characteristic path length means that information has to cross more nodes to reach its final destination [30]. Thus, the decreased global efficiency and increased characteristic path length in the MCAO group suggest a decrease of efficiency in transferring information between nodes in the acute stage after stroke. Besides, we found abnormal nodal efficiency and local efficiency in the acute stage of MCAO, which might affect the normal network organization for transforming and disseminating information among different circuits. The nodes of increased nodal efficiency and local efficiency in the MCAO group also had higher FDG uptake than in the sham group; they were located on the contralesional side and may be involved in functional changes in the acute stage of stroke. In addition, most of the nodes in the MCAO group had decreased nodal efficiency and local efficiency, especially in the ipsilesional striatum. The abnormal properties of the striatum play an important role in the motor dysfunction in the MCAO rat model, while several studies have shown that abnormal motor functions are associated with the abnormal metabolism of neurochemicals in the striatum [44, 45]. Besides, our previous study also showed that motor dysfunction is associated with the abnormal neuronal activity in the striatum revealed by fMRI [9]. Furthermore, the connectivity of the ipsilesional striatum with the ipsilesional cerebellum, ipsilesional hippocampus, and bilateral hypothalamus was decreased based on comparisons of metabolic connectivity. Previous network analyses using fMRI have reported that the striatum shows connectivity to the cerebellum, hippocampus, insular cortex, medial prefrontal cortex, and amygdala, which take part in incentive-based learning, motivation, and action [46, 47]. The cerebellum directs the conscious or volitional motor functions, and several studies have reported abnormal connectivity of the striatum with the cerebellum in motor disorders, such as Parkinson's disease [48]. Studies have shown that the hippocampus plays an important role in the control of some forms of motor activity [49]. The hypothalamus is an essential part of a circuitry that controls motivated behaviors [50]. Studies have shown that dysfunctions of the hippocampus and hypothalamus are associated with the motor dysfunction in stroke [9, 51]. The results suggested an abnormal metabolic connection of the ipsilesional striatum with the ipsilesional

cerebellum, ipsilesional hippocampus, and bilateral hypothalamus in MCAO at the acute stage. Previous studies have demonstrated that improvement of the abnormal brain network contributes to the rehabilitation of the motor function after stroke [52, 53]. The abnormal metabolic connections might provide insight into the treatment of patients with motor dysfunction after stroke.

In addition, some limitations in our work need to be pointed out. First, any disturbance might affect brain function, which could affect the FDG-PET images. In order to minimize animal suffering, the behavioral deficits of the MCAO group were not evaluated. According to previous studies, neurological deficits in the MCAO group occur at 2 h after ischemic stroke [54, 55]. Based on the FDG-PET images and our previous studies [54, 55], neurological functions in the MCAO group were decreased at 12 h after stroke. Further studies should be done to validate the results. Second, in consideration of the spatial resolution of the PET images, only nodes which were large enough were selected in the study; more detailed nodes should be selected for further study.

In conclusion, based on FDG-PET, we demonstrated abnormal metabolic connectivity in the MCAO rat at the acute stage. Not only the global and regional graph theoretic properties but also the functional correlations were significantly different between the MCAO and sham groups, particularly involving the metabolic connections of the striatum.

Acknowledgements This work was supported by grants from the National Natural Science Foundation of China (81471741, 81471728, and 81671770).

Compliance with Ethical Standards

Conflict of interest The authors declare that they have no conflict of interest.

References

1. Feigin VL, Forouzanfar MH, Krishnamurthi R, Mensah GA, Connor M, Bennett DA, *et al.* Global and regional burden of stroke during 1990–2010: findings from the Global Burden of Disease Study 2010. Lancet 2014, 383: 245–255.
2. Langhorne P, Coupar F, Pollock A. Motor recovery after stroke: a systematic review. Lancet Neurol 2009, 8: 741–754.
3. Chamorro Á, Dirnagl U, Urra X, Planas AM. Neuroprotection in acute stroke: targeting excitotoxicity, oxidative and nitrosative stress, and inflammation. Lancet Neurol 2016, 15: 869–881.
4. Johnston SC, Amarenco P, Albers GW, Denison H, Easton JD, Evans SR, *et al.* Ticagrelor versus aspirin in acute stroke or transient ischemic attack. N Engl J Med 2016, 375: 35–43.
5. Powers WJ, Derdeyn CP, Biller J, Coffey CS, Hoh BL, Jauch EC, *et al.* 2015 American Heart Association/American Stroke Association Focused Update of the 2013 Guidelines for the Early Management of Patients With Acute Ischemic Stroke Regarding Endovascular Treatment: A Guideline for Healthcare Professionals From the American Heart Association/American Stroke Association. Stroke 2015, 46: 3020–3035.
6. Yao QL, Zhang HY, Nie BB, Fang F, Jiao Y, Teng GJ. MRI assessment of amplitude of low-frequency fluctuation in rat brains with acute cerebral ischemic stroke. Neurosci Lett 2012, 509: 22–26.
7. Ding X, Li CY, Wang QS, Du FZ, Ke ZW, Peng F, *et al.* Patterns in default-mode network connectivity for determining outcomes in cognitive function in acute stroke patients. Neuroscience 2014, 277: 637–646.
8. Park CH, Chang WH, Ohn SH, Kim ST, Bang OY, Pascual-Leone A, *et al.* Longitudinal changes of resting-state functional connectivity during motor recovery after stroke. Stroke 2011, 42: 1357–1362.
9. Liang S, Lin Y, Lin B, Li J, Liu W, Chen L, *et al.* Resting-state functional magnetic resonance imaging analysis of brain functional activity in rats with ischemic stroke treated by electroacupuncture. J Stroke Cerebrovasc Dis 2017, 26: 1953–1959.
10. van den Heuvel MP, Hulshoff Pol HE. Exploring the brain network: a review on resting-state fMRI functional connectivity. Eur Neuropsychopharmacol 2010, 20: 519–534.
11. Li B, Cui LB, Xi YB, Friston KJ, Guo F, Wang HN, *et al.* Abnormal effective connectivity in the brain is involved in auditory verbal hallucinations in schizophrenia. Neurosci Bull 2017, 33: 281–291.
12. Yakushev I, Drzezga A, Habeck C. Metabolic connectivity: methods and applications. Curr Opin Neurol 2017, 30: 677–685.
13. Gorges M, Roselli F, Muller HP, Ludolph AC, Rasche V, Kassubek J. Functional connectivity mapping in the animal model: principles and applications of resting-state fMRI. Front Neurol 2017, 8: 200.
14. Zou N, Chetelat G, Baydogan MG, Li J, Fischer FU, Titov D, *et al.* Metabolic connectivity as index of verbal working memory. J Cereb Blood Flow Metab 2015, 35: 1122–1126.
15. Chung J, Yoo K, Kim E, Na DL, Jeong Y. Glucose metabolic brain networks in early-onset vs. late-onset Alzheimer's disease. Front Aging Neurosci 2016, 8: 159.
16. Toussaint PJ, Perlbarg V, Bellec P, Desarnaud S, Lacomblez L, Doyon J, *et al.* Resting state FDG-PET functional connectivity as an early biomarker of Alzheimer's disease using conjoint univariate and independent component analyses. Neuroimage 2012, 63: 936–946.
17. Sala A, Caminiti SP, Presotto L, Premi E, Pilotto A, Turrone R, *et al.* Altered brain metabolic connectivity at multiscale level in early Parkinson's disease. Sci Rep 2017, 7: 4256.
18. Caliandro P, Vecchio F, Miraglia F, Reale G, Della Marca G, La Torre G, *et al.* Small-world characteristics of cortical connectivity changes in acute stroke. Neurorehabil Neural Repair 2017, 31: 81–94.
19. Philips GR, Daly JJ, Principe JC. Topographical measures of functional connectivity as biomarkers for post-stroke motor recovery. J Neuroeng Rehabil 2017, 14: 67.
20. Zhu Y, Bai L, Liang P, Kang S, Gao H, Yang H. Disrupted brain connectivity networks in acute ischemic stroke patients. Brain Imaging Behav 2017, 11: 444–453.
21. Longa EZ, Weinstein PR, Carlson S, Cummins R. Reversible middle cerebral artery occlusion without craniectomy in rats. Stroke 1989, 20: 84.
22. Matsumura A, Mizokawa S, Tanaka M, Wada Y, Nozaki S, Nakamura F, *et al.* Assessment of microPET performance in analyzing the rat brain under different types of anesthesia: comparison between quantitative data obtained with microPET and ex vivo autoradiography. Neuroimage 2003, 20: 2040–2050.
23. Nie B, Chen K, Zhao S, Liu J, Gu X, Yao Q, *et al.* A rat brain MRI template with digital stereotaxic atlas of fine anatomical

delineations in paxinos space and its automated application in voxel-wise analysis. Hum Brain Mapp 2013, 34: 1306–1318.
24. Nie B, Liu H, Chen K, Jiang X, Shan B. A statistical parametric mapping toolbox used for voxel-wise analysis of FDG-PET images of rat brain. PLoS One 2014, 9: e108295.
25. Liang S, Wu S, Huang Q, Duan S, Liu H, Li Y, *et al.* Rat brain digital stereotaxic white matter atlas with fine tract delineation in Paxinos space and its automated applications in DTI data analysis. Magn Reson Imaging 2017, 43: 122–128.
26. Paxinos G, Watson C. The rat brain in stereotaxic coordinates 5th edition. New York: Academic Press 2005.
27. Nie B, Liang S, Jiang X, Duan S, Huang Q, Zhang T, *et al.* Automatic method for generating an unbiased intensity normalizing factor in positron emission tomography image analysis after stroke. Neurosci Bull, 2018. https://doi.org/10.1007/s12264-018-0240-8.
28. Kaiser M. A tutorial in connectome analysis: topological and spatial features of brain networks. Neuroimage 2011, 57: 892–907.
29. Choi H, Kim YK, Kang H, Lee H, Im HJ, Hwang DW, *et al.* Abnormal metabolic connectivity in the pilocarpine-induced epilepsy rat model: a multiscale network analysis based on persistent homology. Neuroimage 2014, 99: 226–236.
30. Rubinov M, Sporns O. Complex network measures of brain connectivity: uses and interpretations. Neuroimage 2010, 52: 1059–1069.
31. Achard S, Bullmore E. Efficiency and cost of economical brain functional networks. PLoS Comput Biol 2007, 3: e17.
32. Cha J, Kim ST, Jung WB, Han YH, Im GH, Lee JH. Altered white matter integrity and functional connectivity of hyperacute-stage cerebral ischemia in a rat model. Magn Reson Imaging 2016, 34: 1189–1198.
33. Mohajerani MH, Aminoltejari K, Murphy TH. Targeted mini-strokes produce changes in interhemispheric sensory signal processing that are indicative of disinhibition within minutes. Proc Natl Acad Sci U S A 2011, 108: E183–E191.
34. Erlich JC, Bialek M, Brody CD. A cortical substrate for memory-guided orienting in the rat. Neuron 2011, 72: 330–343.
35. Xu Q, Yang JW, Cao Y, Zhang LW, Zeng XH, Li F, *et al.* Acupuncture improves locomotor function by enhancing GABA receptor expression in transient focal cerebral ischemia rats. Neurosci Lett 2015, 588: 88–94.
36. Coull JT, Hwang HJ, Leyton M, Dagher A. Dopamine precursor depletion impairs timing in healthy volunteers by attenuating activity in putamen and supplementary motor area. J Neurosci 2012, 32: 16704–16715.
37. Bedard P, Sanes JN. Brain representations for acquiring and recalling visual-motor adaptations. Neuroimage 2014, 101: 225–235.
38. Tang WK, Liang HJ, Chen YK, Chu WC, Abrigo J, Mok VC, *et al.* Poststroke fatigue is associated with caudate infarcts. J Neurol Sci 2013, 324: 131–135.
39. Jang SH. Recovery mechanisms of somatosensory function in stroke patients: implications of brain imaging studies. Neurosci Bull 2013, 29: 366–372.
40. Ward NS, Brown MM, Thompson AJ, Frackowiak RSJ. Neural correlates of motor recovery after stroke: a longitudinal fMRI study. Brain 2003, 126: 2476–2496.
41. Alia C, Spalletti C, Lai S, Panarese A, Lamola G, Bertolucci F, *et al.* Neuroplastic changes following brain ischemia and their contribution to stroke recovery: novel approaches in neurorehabilitation. Front Cell Neurosci 2017, 11: 76.
42. Mansoori BK, Jean-Charles L, Touvykine B, Liu A, Quessy S, Dancause N. Acute inactivation of the contralesional hemisphere for longer durations improves recovery after cortical injury. Exp Neurol 2014, 254: 18–28.
43. Khedr EM, Abdel-Fadeil MR, Farghali A, Qaid M. Role of 1 and 3 Hz repetitive transcranial magnetic stimulation on motor function recovery after acute ischaemic stroke. Eur J Neurol 2009, 16: 1323–1330.
44. Holmes WM, Lopez-Gonzalez MR, Gallagher L, Deuchar GA, Macrae IM, Santosh C. Novel MRI detection of the ischemic penumbra: direct assessment of metabolic integrity. NMR Biomed 2012, 25: 295–304.
45. Berthet C, Xin L, Buscemi L, Benakis C, Gruetter R, Hirt L, *et al.* Non-invasive diagnostic biomarkers for estimating the onset time of permanent cerebral ischemia. J Cereb Blood Flow Metab 2014, 34: 1848–1855.
46. Zhang S, Hu S, Chao HH, Li CR. Hemispheric lateralization of resting-state functional connectivity of the ventral striatum: an exploratory study. Brain Struct Funct 2017, 222: 2573–2583.
47. Tanaka S, Kirino E. Functional connectivity of the dorsal striatum in female musicians. Front Hum Neurosci 2016, 10: 178.
48. Wang Z, Guo Y, Myers KG, Heintz R, Peng YH, Maarek JM, *et al.* Exercise alters resting-state functional connectivity of motor circuits in parkinsonian rats. Neurobiol Aging 2015, 36: 536–544.
49. Vanderwolf CH. The hippocampus as an olfacto-motor mechanism: were the classical anatomists right after all? Behav Brain Res 2001, 127: 25–47.
50. Hurley SW, Johnson AK. The role of the lateral hypothalamus and orexin in ingestive behavior: a model for the translation of past experience and sensed deficits into motivated behaviors. Front Syst Neurosci 2014, 8: 216.
51. Brisson CD, Andrew RD. A neuronal population in hypothalamus that dramatically resists acute ischemic injury compared to neocortex. J Neurophysiol 2012, 108: 419–430.
52. Fan YT, Wu CY, Liu HL, Lin KC, Wai YY, Chen YL. Neuroplastic changes in resting-state functional connectivity after stroke rehabilitation. Front Hum Neurosci 2015, 9: 546.
53. Ripolles P, Rojo N, Grau-Sanchez J, Amengual JL, Camara E, Marco-Pallares J, *et al.* Music supported therapy promotes motor plasticity in individuals with chronic stroke. Brain Imaging Behav 2016, 10: 1289–1307.
54. Tao J, Zheng Y, Liu W, Yang S, Huang J, Xue X, *et al.* Electroacupuncture at LI11 and ST36 acupoints exerts neuroprotective effects via reactive astrocyte proliferation after ischemia and reperfusion injury in rats. Brain Res Bull 2016, 120: 14–24.
55. Liu W, Wang X, Zheng Y, Shang G, Huang J, Tao J, *et al.* Electroacupuncture inhibits inflammatory injury by targeting the miR-9-mediated NF-kappaB signaling pathway following ischemic stroke. Mol Med Rep 2016, 13: 1618–1626.